Reliability based design optimization for bridge girder shape and plate thicknesses of long-span suspension bridges considering flutter constraint

Ibuki Kusano*, Miguel Cid Montoya, Aitor Baldomir, Félix Nieto, José Ángel Jurado, Santiago Hernández

Structural Mechanics Group, School of Civil Engineering, Universidade da Coruña, Campus de Elvina, 15071, A Coruña, Spain

*Corresponding author. Tel.: +34 981 167000 x6030; fax: +34 981 167 170

E-mail address: ibuki.kusano@uis.no (Ibuki Kusano)

Abstract:

Reliability based design optimization (RBDO) for deck shape and thicknesses of the steel plates that form a box girder of long-span suspension bridges is performed considering probabilistic flutter constraint. The entire process was carried out fully computationally including the definition of flutter derivatives. Surrogate models were constructed to estimate the aerodynamic response of the bridge for different deck shapes based on the results from a series of CFD simulations. Some of the aerodynamic coefficients were validated by wind tunnel tests. Flutter derivatives were then estimated using quasi-steady approach for the evaluation of critical flutter velocity. Uncertainty in the aerodynamic coefficients from CFD simulations as well as the extreme wind speed at the bridge site were considered. The formulated methodology was applied to the Great Belt East Bridge.

Keywords: *RBDO; shape optimization; reliability analysis; flutter derivatives; random variables; suspension bridge; surrogate model; CFD simulation; force coefficients*

1 Introduction

Long-span suspension bridges are flexible structures and thus vulnerable to wind-induced vibrations. Flutter instability is one of the most important among these phenomena for the design since it may cause the collapse of structures. According to Ge (2016), some of the prominent bridges, such as the Akashi Kaikyo Bridge, the Xihoumen Bridge, the Yi Sunsen Bridge, the Jiangsu Runyang Bridge and the Tsing Ma Bridge, had flutter as the principal wind-induced vibration problem. Other wind effects such as buffeting and vortex-induced vibrations are also relevant since they may cause fatigue damage to the structure. The choice of deck shape, therefore, is very important for the design of a suspension bridge since it affects the dynamic response of the structure against

wind-induced instabilities. Diana et al. (2013) underlined the importance of the deck shape on vortex shedding phenomenon while Ge et al. (2008) studied the importance of deck section on flutter velocity for cable-supported bridges. Among various types of bridge decks, the stream-lined box girder became popular after its successful application to the Severn Bridge in Great Britain in 1966, and it has been widely used all over the world mainly because of its good performance against vortex shedding and flutter instabilities. The box sections provide larger torsional inertia than open sections, the deck can be designed shorter in height, which results in more slender and aesthetic appearance. The box section is also more economic in construction as well as corrosion maintenance (Gimsing and Georgakis, 2012).

Computation of aeroelastic and aerodynamic responses in cable-supported bridges depends on non-deterministic parameters that can be treated by reliability analysis methods. There are many researchers who have worked on uncertainty in aerodynamic and aeroelastic forces on deck sections of cable supported bridges. Ostenfeld-Rosenthal et al. (1992) considered experimentally obtained flutter derivatives as Gaussian random variables and performed First Order Reliability Method (FORM) considering four random variables. Ge et al. (2000) presented a method to obtain probability of failure against flutter using FORM, in which empirical flutter formula was used to define the limit state. Sarkar et al. (2009) compared experimentally obtained flutter derivatives results from different laboratories and examined the implications of dissimilarities among flutter derivative data sets on the aeroelastic instability of long-span bridges. Caracoglia et al. (2009) reported the nonlinear propagation of an uncertain turbulence field on the aeroelastic stability of long-span bridges. Baldomir et al. (2013) performed reliability analysis of long-span bridges considering uncertainty in flutter derivatives, extreme wind speed and structural damping. Seo (2013) proposed a statistics-based method for buffeting analysis considering uncertainty in flutter derivatives. Argentini et al. (2014) studied the effects of mechanical and aerodynamic uncertainty on total damping and flutter speed while Thomas et al. (2015) proposed stochastic bridge flutter formulation in random eigenvalue analysis.

In the case of critical flutter velocity computation based on experimentally obtained flutter derivatives as in our previous researches (Kusano et al. 2014, 2015), the uncertainty may come from laboratory environment or operational conditions as well as the techniques used to extract the data. In the case of critical flutter evaluation based on

the data from computational fluid dynamic (CFD) simulations, uncertainty may result from the boundary conditions, grid size, choice of turbulence model and so on. In either method, the consideration of uncertainty in the estimation of critical flutter velocity is important.

Since one of the major expenses for the construction of long-span bridges is the material costs, it is of great importance to reduce material weight in today's highly competitive economic environment. The use of design optimization permits the reduction of materials while satisfying required structural constraints (Hernández, 1990; Arora, 2016). Compared to the traditional deterministic optimization, the reliability based design optimization (RBDO) seeks the optimum design considering uncertainties in parameters, which makes this method more robust and accurate. The material cost is minimized subject to prescribed probabilistic constraints, in which engineers should set a predetermined reliability level. This value is known as the target reliability index, β^T, which is defined as $\beta^T = \Phi^{-1}(1-P_f)$ where P_f is the probability of failure that a designer is willing to accept.

There have been many applications of the RBDO to different structures mainly in aerospace, defense, automobile and offshore structures. See, for example, Marvis (1999), Yao (2011), Karadeniz (2009) or Youn et al. (2004). However, there have been very few RBDO application to civil structures, especially to suspension bridges. In our previous works, Kusano et al. (2014, 2015) performed the RBDO of the steel plate thicknesses that form box girders and the main cable area for suspension bridges under probabilistic flutter constraint, in which experimentally obtained flutter derivatives and extreme wind velocity were considered as random variables while Kusano et al. (2018) reported the importance of correlation among experimentally obtained flutter derivatives on the critical flutter velocity. Cid Montoya et al. (2018a, 2018b) carried out deterministic optimization of deck shape for cable-stayed bridges considering aeroelastic constraint, in which aerodynamic surrogate models were constructed based on CFD simulation models. Knowing that the deck shape is very important to control the aeroelastic behavior of suspension bridges, we extend our research of the RBDO to perform the shape optimization as well as the size optimization of a single box girder for suspension bridges under probabilistic flutter constraint. For Runyang Bridge in China (Chen et al., 2002), a central stabilizer was installed to control flutter instability; however, this problem may have been solved by adapting another deck shape using, for example, the framework

proposed in this study. Other wind-induced phenomena such as buffeting, which is associated with deck plate size and fatigue problem as well as vortex-induced vibrations will be included in our forthcoming works since they are relevant to the deck design.

In order to achieve this objective, a fully numerical approach for the definition of flutter derivatives is essential to compute the critical flutter velocity for each modified deck section during the optimization process. A series of Computational Fluid Dynamics (CFD) simulations were conducted to obtain aerodynamic force coefficients of different deck sections. Subsequently, aerodynamic surrogate models were constructed based on the CFD results in order to estimate the force coefficients of different deck sections (Cid Montoya et al., 2018a). Then quasi-steady formulation was employed to define flutter derivatives in terms of these force coefficients. Uncertainty in the force coefficients and their slopes as well as the extreme wind velocity at the bridge location was considered in the definition of bridge flutter limit state. Finally, the RBDO methodology was applied to the Great Belt East Bridge using Reliability Index Approach (RIA) method.

The main objectives of this research can be summarized as follows.

- Definition of fully numerical approach of critical flutter velocity computation based on a series of CFD simulations and aerodynamic surrogate models.
- Reliability analyses of suspension bridges considering uncertainty in the aerodynamic force coefficients and their slopes with respect to the angle of attack obtained from CFD as well as the extreme wind speed.
- RBDO for shape and size of a box girder of suspension bridges under probabilistic flutter constraint considering uncertainty in the parameters mentioned above.

2 Computation of flutter velocity using quasi-steady model

There are currently three major approaches to compute flutter velocity of cable-supported bridges: fully experimental, fully computational or hybrid method of these two approaches. For both fully experimental and hybrid methods, expensive and time-consuming wind tunnel tests of either entire bridge or sectional models are required. On the other hand, the fully-computational approach permits the substitution of sectional model tests by equivalent numerical simulations (Larsen and Walther, 1998).

For the execution of shape design optimization of a bridge deck, this fully numerical approach is crucial since it is impractical to test every possible deck shapes in the wind tunnel during the optimization process. The fully computational method for the estimation of critical flutter speed employed in this research is briefly described in this section.

The wind loads acting on a unit-length of a static bridge deck subject to a constant wind, which is commonly known as the steady load model, can be defined as three components of lift, drag and moment. They may be expressed as non-dimensional time-averaged quantities called force coefficients, which are functions of wind attack angle to the deck cross-section as:

$$C_L = \frac{L}{0.5 \cdot \rho U^2 B};\ C_D = \frac{D}{0.5 \cdot \rho U^2 B};\ C_M = \frac{M}{0.5 \cdot \rho U^2 B^2} \tag{1}$$

where C_L, C_D and C_M are lift, drag and moment coefficients, L, D and M are the time-averaged lift and drag forces and moment per unit of length, ρ is the flow density, U is the undisturbed wind velocity and B is the width of the deck cross-section. The force scheme and the sign convection adopted in the study are shown in Figure 1.

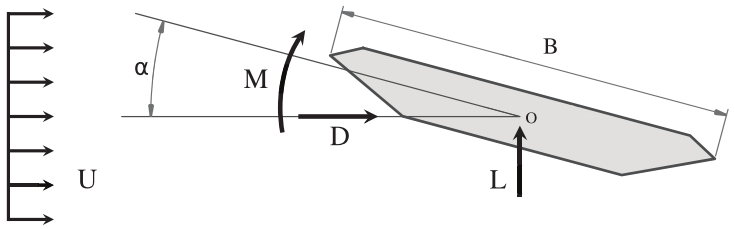

Figure 1. Definition of the steady load model with the three aerodynamic steady force components and the sign convection adopted

When displacements of the deck are considered, a more sophisticated load model is required. Scanlan and Tomko (1971) established the semi-empirical approach which consists of the definition of frequency dependent unsteady functions known as flutter derivatives from aeroelastic wind-tunnel sectional tests to define the three aeroelastic force components as:

$$\mathbf{f}_a = \begin{Bmatrix} D_a \\ L_a \\ M_a \end{Bmatrix} = \frac{1}{2}\rho UKB \cdot \begin{pmatrix} P_1^* & -P_5^* & -BP_2^* \\ -H_5^* & H_1^* & BH_2^* \\ -BA_5^* & BA_1^* & B^2A_2^* \end{pmatrix} \begin{Bmatrix} \dot{v} \\ \dot{w} \\ \dot{\varphi}_x \end{Bmatrix} + \frac{1}{2}\rho U^2 K^2 \cdot \begin{pmatrix} P_4^* & -P_6^* & -BP_3^* \\ -H_6^* & H_4^* & BH_3^* \\ -BA_6^* & BA_4^* & B^2A_3^* \end{pmatrix} \begin{Bmatrix} v \\ w \\ \varphi_x \end{Bmatrix} \tag{2}$$

where B is the deck width, U is the acting wind speed, $K = B\omega/U$ is the reduced frequency with ω as the response frequency, A_i^*, H_i^* and P_i^* (i=1,…,6) are the flutter derivatives obtained experimentally.

However, in order to estimate the flutter derivatives numerically to avoid the expensive wind tunnel tests, an alternative approach is required. The quasi-steady wind load model improves the steady wind load model by considering the displacements of the deck and the turbulent nature of the natural wind, giving place to a two-dimensional framework that relates the bridge displacements and rotations with the relative wind velocity components. The resulting formulation is adequate for high reduced wind velocities and streamlined deck cross-sections as discussed in Tubino (2005) and Wu and Kareem (2013). Once this model is linearized (Lazzari, 2005), the resulting expressions of aeroelastic forces are functions of displacements and their derivatives of the deck as well as force coefficients and their slopes. By comparing the wind loads obtained from the quasi-steady wind load model and Scanlan's model, flutter derivatives can be defined in terms of force coefficients as follows:

$$H_1^* = -\frac{C'_{L,0^o} + C_{D,0^o}}{K} \text{ (3a)}; \quad H_2^* = \frac{C'_{L,0^o} + C_{D,0^o}}{K} \cdot \mu_H \text{ (3b)}; \quad H_3^* = -\frac{C'_{L,0^o}}{K^2} \text{ (3c)};$$

$$A_1^* = \frac{C'_{M,0^o}}{K} \text{ (3d)}; \quad A_2^* = \frac{C'_{M,0^o}}{K} \cdot \mu_A \text{ (3e)}; \quad A_3^* = -\frac{C'_{M,0^o}}{K^2} \text{ (3f)}$$

where $C_{L,0^o}$, $C_{D,0^o}$, $C_{M,0^o}$, are lift, drag, and moment coefficients at 0º of angle of attack, $C'_{L,0^o}$, $C'_{D,0^o}$, $C'_{M,0^o}$, are their derivatives while μ_H and μ_A can be estimated according to Larose and Livesey (1997) as:

$$\mu_H \approx \frac{A_1^*}{H_1^*} \text{ and } \mu_A \approx \frac{A_3^*}{H_3^*} \quad (4)$$

The system of equations that governs the dynamic behavior of the deck under aeroelastic forces is expressed as:

$$\mathbf{M\ddot{y} + (C - C_a)\dot{y} + (K - K_a)y = 0} \quad (5)$$

where **M**, **C**, and **K** are mass, damping, and stiffness matrices, and $\mathbf{C}_a$ and $\mathbf{K}_a$ are aeroelastic damping and stiffness matrices, and **y**, $\dot{\mathbf{y}}$ and $\ddot{\mathbf{y}}$ are the vectors of displacements, velocities and accelerations, respectively. Eq. (5) can be solved using multi-modal analysis, which solves the flutter eigenvalue problem. The details of the method can be found in Katsuchi et al. (1999) or Jurado et al. (2004). FLAS program coded in our research group was used to solve this multimodal eigenvalue problem to compute critical flutter velocity throughout the study (Jurado, 2011, 2013, Diana et al, 2019).

3 Uncertainty data in the computation of flutter velocity

There is a series of uncertainty parameters involved in the estimation of critical flutter velocity (see works by Davenport (1983) and Kareem (1988) among others). In the case of widely-employed hybrid method, wind tunnel tests of a bridge sectional model are necessary to obtain flutter derivatives either by free or forced vibration method. Flutter derivatives obtained from such method contains intrinsic uncertainty due to the laboratory environment, operational conditions, uncertainty data such as upstream turbulence, sampling rate as well as techniques used to extract flutter derivatives as reported by Sarkar et al. (2009).

In our previous studies (Baldomir et al. 2013, Kusano et al., 2014, 2015), we considered the points that define flutter derivative functions as normally distributed random variables with the experimental data as mean values to account for uncertainty in flutter derivatives. Flutter velocity was then computed by solving the Eq. (5) through an eigenvalue problem using multi-modal analysis.

In the case of fully numerical approach described in Section 2, flutter derivatives are approximated in terms of force coefficients C_L, C_M and C_D as well as their derivatives C'_L C'_M and C'_D using the quasit-steady formulation in Eq (3). Then flutter velocity is computed by solving Eq. (5) as in the previous case. Now the source of uncertainty in flutter velocity lies in the settings and parameters used to perform the Computational Fluid Dynamics (CFD) simulations. Some of these parameters may be the surface roughness, turbulence length scale and turbulence intensity among others that can be considered as nondeterministic. (Solari and Piccard, 2001 and Bruno and Fransos, 2011). Furthermore, turbulence models based upon the Boussinesq approximation such as the k-ω SST, adopted in this work are affected by uncertainties related with the model assumptions (Gorlé et al. 2015).

In this research, uncertainty is not considered in the input data of the numerical simulations but in the force coefficients obtained through deterministic CFD simulations. The obtained values of force coefficient are taken as the mean values of a new set of random variables where the dispersion and the type of probabilistic distribution are defined. The probabilistic definition of uncertainty in force coefficients has been studied in several works in the last three decades. Some authors have provided guidelines from the probabilistic definition of the force coefficients and other aerodynamic and aeroelastic responses, which are reported in Table 1. Based on these data and bearing in mind that

deck geometry under study is a streamlined cross-section, a normal distribution with a Coefficient of Variation (CV) of 0.2 was adopted for the force coefficients in this study.

Table 1. Uncertainties of aerodynamic and aeroelastic responses of bridge deck cross sections reported in literature

Reference	Substructure/geometry	Response	Distrib.	CV	Source
Cheng & Li (2009)	arch deck cross-section	force coeff.	lognormal	0.2	assumed
Kareem (1988)	tall concrete chimney	drag coeff.	lognormal	0.14	assumed
Bruno & Fransos (2011)	trapezoidal box girder	lift coeff.	truncated Weibull	0.52519	calculated
Pagnini (2010)	tall building	drag coeff.	lognormal	0.1	assumed
Pagnini (2010)	tall building	lift coeff. deriv.	normal	0.1	assumed
Schueller et al.(1983)	tall building	drag coeff.	lognormal	0.15	Rojiani & Wen (1981)
Su (2010)	Ting Kau Bridge deck cross-section	force coeff.	normal	0.1	Liu et al. (2004), Cheng (2005)
Ostenfeld et al. (1992)	Geat Belt East Bridge	model test results	normal	0.05	assumed
Ge et al. (2000)	Yangpu Bridge	model test results	normal	0.05	assumed
Pourzaynail & Datta (2002)	deck cross-section suspension bridge	flutter derivatives	lognormal	0.2	assumed
Cheng et al. (2005)	Jing Yin Bridge	flutter derivatives	lognormal	0.2	Pourzaynail & Datta (2002)

As stated in Eq. (3) flutter derivatives can be expressed in terms of force coefficients and their slopes. Therefore those slopes are also nondeterministic variables whose mean value is the resulting value from the CFD simulation while the standard deviation is computed as:

$$\sigma_{c_i'} = \frac{\sqrt{(\sigma_{c_i 0^o})^2 + (\sigma_{c_i 2^o})^2 + 2\rho \cdot \sigma_{c_i 0^o} \cdot \sigma_{c_i 2^o}}}{\Delta\alpha} \tag{6}$$

where $\sigma_{c_i'}$ is the standard deviation of slope of a force coefficient, $\sigma_{c_i 0^o}$ and $\sigma_{c_i 2^o}$ are the standard deviations of the coefficient at 0 and 2 degrees of angle of attack respectively, ρ is the correlation, and $\Delta\alpha$ is the change in angle in radians. The $\Delta\alpha$ value of 2 degrees is considered since it allows an accurate estimation of the slope in the rectilinear part of the lift and moment coefficients as a function of the angle of attack for considering streamlined geometries.

4 Strategy for the RBDO of shape and size of a box girder

4.1 Introduction

For the construction of long-span bridges, huge material cost is required, in which steel material used for bridge deck and main cables constitute the largest part. Consequently the reduction in material quantity of these elements by carrying out design optimization would be of great importance. Traditionally, civil engineering structures have been built in overly conservative manner in order to deal with uncertainty factors that the structures may suffer during their lifetime using partial safety factors. However, designs based on such approach are not competitive since safety factors do not reflect the random nature of some parameters. RBDO methods allow to optimize structures taking into account uncertainties while satisfying predetermined structural reliability levels referred to one or more limit states. As a result, the RBDO method can provide more economic and reliable designs.

As mentioned previously, deck shape is an important factor that affects the aerodynamic performance of any suspension bridge. In this study, some parameters that define the shape as well as the thicknesses of deck plates were considered as design variables for the RBDO problem under probabilistic flutter constraint. Among the existing RBDO methods, Reliability Index Approach (RIA) proposed by Nikolaidis and Burdisso (1988) was employed in this research, which utilizes the FORM in the reliability routine. This is a two-level method where the design optimization is performed in the outer loop in the original random space (*x*-space) while reliability analysis is carried out in the inner loop in the independent standard normal random space (*u*-space). The reliability index β is defined as the minimum distance from the mean values of the random variables to the failure surface and the reliability analysis using FORM is formulated as:

$$\text{minimize: } \beta = \|\mathbf{u}\| \tag{7a}$$

$$\text{subject to: } G_i(\mathbf{u}) = 0 \tag{7b}$$

This optimization problem can be solved using the Hasofer-Lind algorithm (1974). The solution of this problem $\mathbf{u}^*$ is called the Most Probable Point of failure (MPP) which represents the most probable values of random variables in case of structural failure. Once the MPP is obtained, the reliability index is computed as the distance from the origin in the *U*-space (mean values) to the failure hyperplane.

4.2 Formulation of the RBDO problem

The box girder typology considered in this research is shown in Figure 2, which is based on Scanlan's G1 section (Scanlan and Tomko, 1971). The original dimension is drawn in solid lines while possible shape modifications are shown in broken lines. δH and δB are the shape design variables, which define the changes in height and width with respect to the original dimensions in percent. The top and bottom plate lengths, *a-f* and *c-d*, are fixed while the points *b* and *e* can change their horizontal coordinate to modify the deck width and in the same manner, points *c* and *d* can move vertically to change the deck height. Besides these shape design variables, there are additional design variables of the thicknesses of the steel plates that form the box girder (d_1, d_2, d_3, d_4).

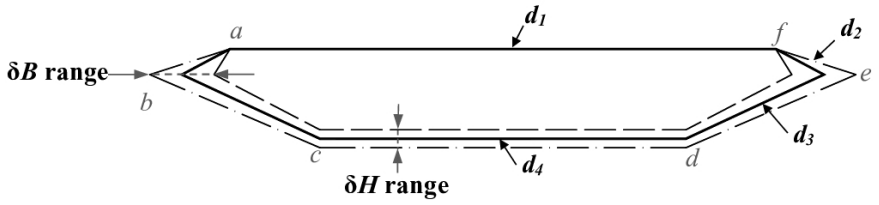

Figure 2. Design variables of the shape and plate thicknesses

The objective is to minimize the material volume of the bridge girder defined by the shape variables of δH and δB and the plate thicknesses, d_1 through d_4. Uncertainties in force coefficients and their derivatives are taken into account along with the extreme wind velocity at the bridge location. The limit state function that defines the structural failure due to flutter is defined as:

$$G(\mathbf{x}) = V_f(x_i) - x_w \qquad i=1, 2, \ldots, 6 \tag{8}$$

where V_f is the flutter wind speed of the bridge, x_i are 6 random variables of the force coefficients and their slopes, and x_w is the random variable of the extreme wind speed at the bridge location.

It should be mentioned that all six design variables are involved in the evaluation of this limit state function. The shape design variables define flutter derivatives based on the force coefficients while the size variable of each plate thickness affects the stiffness of the structure, thus influencing the frequencies and mode shape of the structure. Consequently, the reliability of the structure against flutter depends on both shape and size design variables as well as the random variables.

Then the RBDO problem is formulated as:

$$\text{Minimize:} \quad \text{Girder volume } (\delta H, \delta B, d_1, d_2, d_3, d_4) \tag{9a}$$

$$\text{subject to:} \quad g_1 : P\left[V_f(\mathbf{x}) - x_w \le 0\right] \le P_f \tag{9b}$$

$$g_2 : \delta H_{\min} \le \delta H \le \delta H_{\max} \tag{9c}$$

$$g_3 : \delta B_{\min} \le \delta B \le \delta B_{\max} \tag{9d}$$

$$g_4 : \mathrm{t}_{\min} \le d_j \le \mathrm{t}_{\max} \qquad j = 1, 2, 3, 4 \tag{9e}$$

$$g_5 : \sigma_c = \sigma_{\max} \tag{9f}$$

$$g_6 : \frac{z_d}{z_{\max}} - 1 \le 0 \tag{9g}$$

where **x** is the vector of the random variables of the force coefficients and their slopes, P, the probability operator, P_f, allowable probability of failure, the design variables are restricted by the side limits, σ_c, the maximum tensile stress in the main cable under static overload case, z_d, the maximum vertical mid-span deck displacement under the static overload cases, and z_{max}, the limiting displacement value. The constraint g_1 is probabilistic while the rest of the constraints are deterministic. The probability of flutter failure is evaluated such that reliability index, β, computed in reliability analysis of each iteration is checked against the predetermined target reliability, β^T. The g_5 assigns an appropriate main cable area whenever the deck weight changes so that the maximum cable stress under the static overload case is at a reasonable value, which will be explained in detail in Section 5.5.1 of the application example.

4.3 Surrogate modeling of the aerodynamic responses

Surrogate models allow to reproduce the response of a complex implicit model known as truth or real model, which in this case are the CFD simulations by an analytical approximation known as meta-model or surrogate model. They permit the reduction in computational time of real models for recursive analyses and the obtainment of intermediate designs among those used in the sampling process. Further insights about these models and their use in optimization-related frameworks can be found in Forrester et al. (2008) and Forrester and Keane (2009) while their specific use in reliability analysis and RBDO related works can be found in Martins Gomes and Awruch (2004), Martins Gomes et al. (2011) and Díaz et al. (2016) among many others.

In the problem formulated in Eq. (9), two shape design variables were defined, which require new CFD simulations each time these variables are modified by the optimization algorithm. Since the high computational burden of CFD analyses represents a strong limitation to its systematic recursive use, a surrogate model is defined to obtain the required responses for the reduction in computational effort. The aerodynamic surrogate model used in this work consists of a Kriging model (Krige, 1951, Sacks et al., 1989, Simpson and Mistree 2001) with two inputs of width and depth parameters δB and δH of the section and six outputs of the three force coefficients and theirs slopes. For the application example presented in this research we have used the surrogate model presented in our previous studies (Cid Montoya et al., 2018a, and 2018b), in which CFD results were validated with wind tunnel data and the sensitivity of force coefficients with respect to δB and δH are discussed. The implementation of the aerodynamic surrogate model within the RBDO framework is developed in the following section.

4.4 RBDO procedure

The RBDO problem consists of two main blocks of design optimization and reliability analysis. These two phases are nested in RIA method used in this study, whose work flow is represented in Figure 3. Whenever the optimization algorithm modifies the design variables of the girder shape and plate thicknesses, the MATLAB main code carries out the following main tasks in the design optimization phase. The procedure of the RBDO process can be summarized in the following steps:

1. Compute the mechanical properties of the deck section with updated design variables and modify the FEM input file (area, inertias etc.)
2. Compute the main cable area according to the constraint g_4
3. Using the Abaqus cable model, perform an iterative process to determine the initial main cable length and initial stress so that the cable is positioned as designed. This process is iterative because the mid-span position under the main cable self-weight is unknown although the final mid-span position is known. This step is necessary since any variation in the girder plate thicknesses affects both the initial main cable length and the initial stress, which consequently modify the stiffness of the entire structure.
4. Write Abaqus input files to modify deck properties, initial position and initial stresses of the main and hanger cables, etc.

5. Perform Abaqus nonlinear static analysis to compute the initial stress of the entire bridge under self-weight, whose stiffness matrix is used for the subsequent modal analysis.
6. Carry out a modal analysis to obtain natural frequencies and mode shapes of the bridge and simultaneously run a static analysis to get the maximum vertical displacement under the static overload case. These tasks are performed in parallel.
7. Call the surrogate models with the current shape design of δH and δB to obtain the force coefficients and their derivatives, which are the mean values of random variables in the following reliability analysis.
8. Use the mean values as the initial values of MPP for the first iteration. Otherwise define the random variables x_i and x_w according to the updated normalized variable u_i and u_w, the mean values and the standard deviations.
9. Define flutter derivatives according to the updated force coefficients and their slopes using quasi-steady formulation.
10. Compute the limit state function $G(\mathbf{u})$, and its gradients with respect to each random variable. After β is calculated, the next MPP point is defined. The step 8-10 is repeated until the convergence criteria for reliability analysis are satisfied, which are the relative error between two consecutive β and the value of the limit state function.
11. The converged β from the reliability analysis is checked against the probability constraint, β^{T}, along with other deterministic constraints in the design optimization. Finally the optimization algorithm modifies the design and the step 1-11 is repeated until the convergence criteria are reached, which are set on the relative error between two consecutive objective functions and constraint functions.

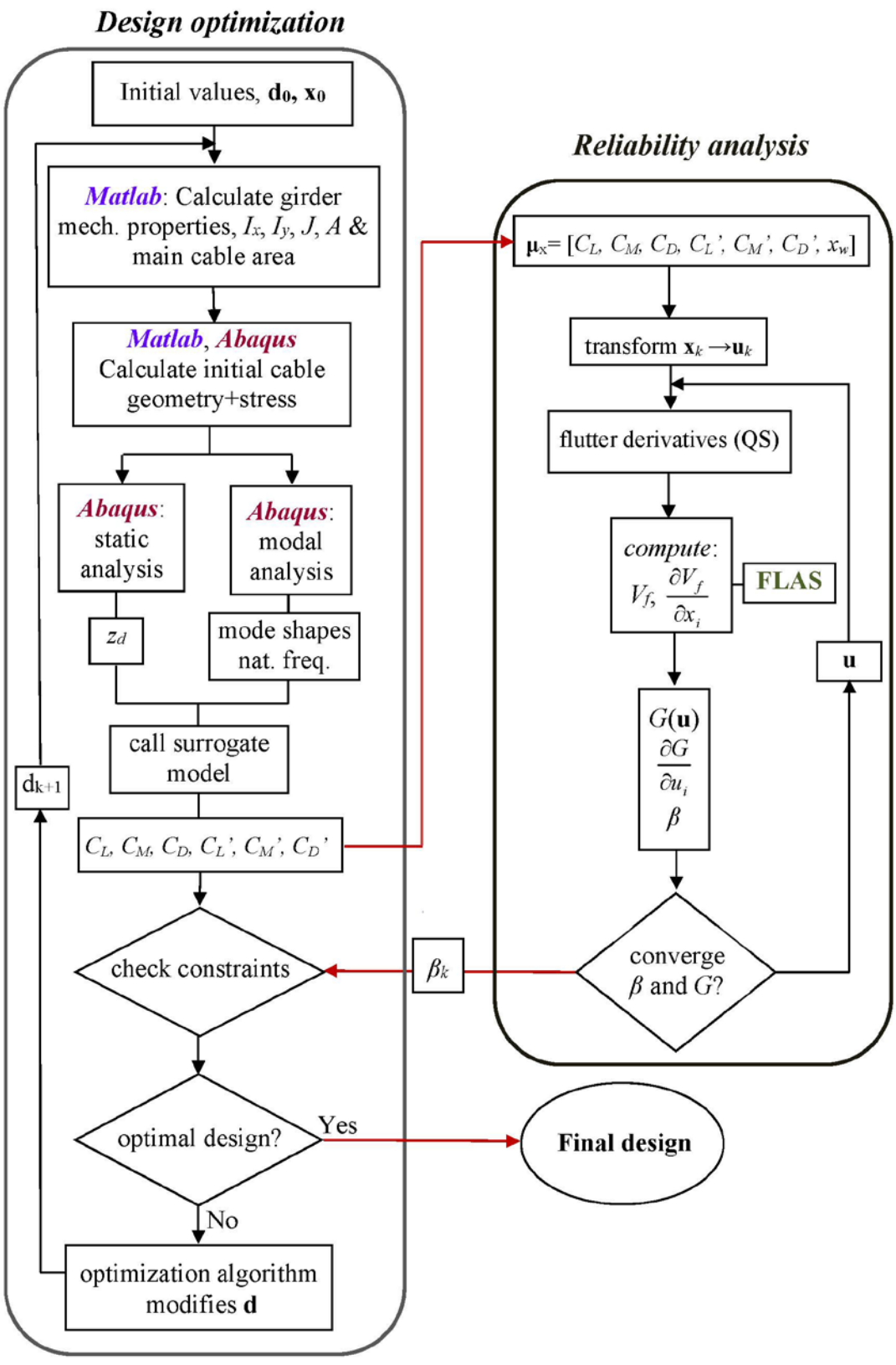

Figure 3. Flowchart of the RBDO strategy

5 Application example: Great Belt East Bridge

5.1 Great Belt East Bridge description

The methodology of RBDO explained in the previous sections is now applied to the Great Belt East Bridge in Denmark. It consists of a main span of 1624 meters and two pylons of 254 meter high as shown in Figure 4. The aerodynamic box girder of the G1 section was employed as a baseline geometry for the deck, which is subject to shape and size optimization. A 3D beam finite element model in Abaqus (2015) in Figure 5 was used to perform both modal and static analyses of the bridge during the optimization. The model consists of 1257 elements and 747 nodes. The bridge deck contains 225 nodes in total, approximately 12 meters apart from one another. The boundary conditions were imposed at the tower foundations and the anchorages. The deck is continuous throughout the three spans without any vertical support while it counts with lateral support at the pylons. The main cables have fixed connections to the girder at the mid span, which helps to minimize deflections under asymmetric loads as described in Storebælt (1998). The initial deck design is shown in Figure 6 while the mechanical properties of the structural model are summarized in Table 2.

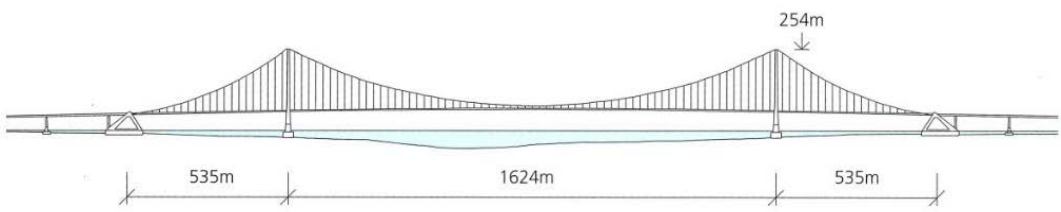

Figure 4. Side view of the Great Belt East Bridge

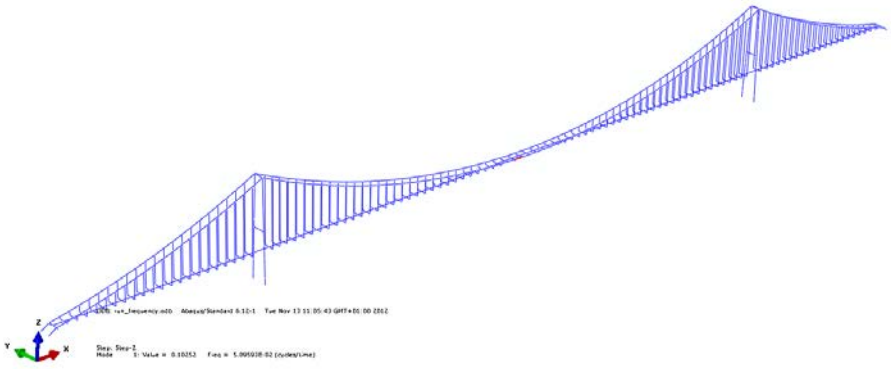

Figure 5. Finite element model of the Great Belt Bridge

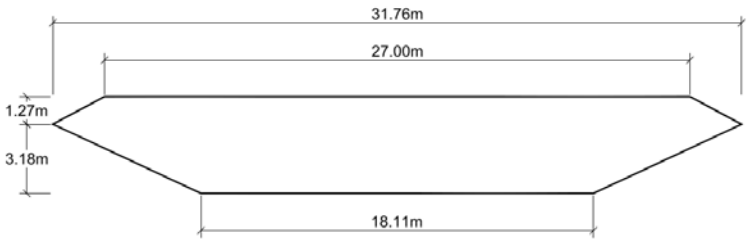

Figure 6. Initial design of the box girder

Table 2. Geometric and mechanical properties of the finite element model of the initial design

Property	Value	Property	Value
Center span length (m)	1624	Deck height (m)	4.447
Lateral span length (m)	535	Deck moment of inertia, I_y (m^4)	3.926
Main cable sag (m)	180	Deck moment of inertia, I_z (m^4)	73.200
Distance between main cables (m)	27	Deck polar moment of inertia, J (m^4)	8.896
Pylon height (m)	254	Mass per unit length of deck (t/m)	14.750
Total deck width (m)	31.765	Main cable cross sectional area (m^2)	0.449

5.2 Critical flutter velocity of the initial design

First of all, the natural frequencies and the mode shapes of the bridge were computed using the Abaqus finite element model. Because of the large flexibility of the structure, the modal analysis was performed in two steps. In the first step, the initial stresses of the main cables and vertical hanger cables were computed under the self-weight, and in the subsequent step, modal analysis was performed with the overall stiffness of the structure. Table 3 lists the natural frequencies and the vibration modes of the initial design of the bridge deck obtained by the authors, which were then compared to the values reported by Larsen (1993).

Table 3. Natural frequencies and vibration modes of the initial design: L (lateral), V (vertical), T (torsional), S (symmetric), A (asymmetric)

Mode	Type	present work	Larsen	Mode	Type	present work	Larsen
1	LS	0.050	0.052	15	VS	0.216	
2	VS	0.098	0.100	18	VS	0.249	
3	VA	0.111	0.115	19	LA	0.275	
4	LA	0.113	0.123	20	VS	0.282	
5	VS	0.131	0.135	21	TS/LS	0.285	0.278
8	VA	0.177		22	VS	0.285	
9	LA	0.184		23	VA	0.286	
10	VA	0.186		24	TS/LS	0.290	
11	LS	0.186	0.187	25	LA	0.295	
12	LS	0.195		28	LA	0.327	
13	LA	0.213		29	LS	0.329	
14	LS	0.213		30	LS	0.335	

In the next step, several relevant modes were selected for performing flutter analyses. After carrying out a series of test runs, we identified several essential modes in the flutter analysis such as the first, second, third and fourth vertical symmetric modes as well as the first and second torsional symmetric modes. In order to cover the changes in vibration modes during the optimization process, we have selected 20 modes, mode 2, 5 and 11 through 28 to be used for flutter analysis. As commented in Section 2, FLAS program coded in our research group was employed for the aeroelastic analysis in this research. Figure 7 shows the result of flutter analysis with the initial design of the G1 deck section. Flutter is produced at the wind velocity of 78.20 m/s and the reduced frequency of 0.477.

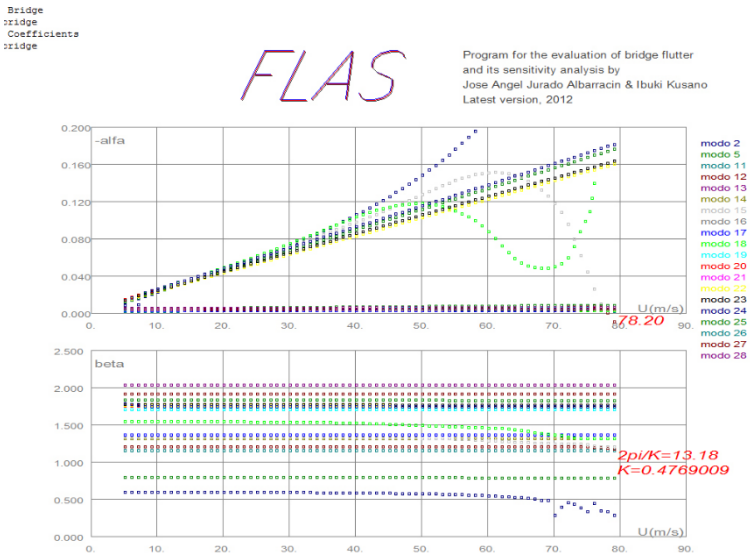

Figure 7. Flutter result for the initial deck design

5.3 Parametric study of flutter velocity for different deck shapes

A parametric study was carried out to see how flutter velocity changes for different values of shape variables. Figure 8 shows the design domain of δH and δB, which can be varied from -10% to 10% of their nominal values. The resulting flutter velocities by varying the shape variables are plotted in Figure 9. As can be seen, there is a smooth shape of steady flutter velocity between δB +10% and δB -4%; however, the flutter velocity decreases rapidly from δB -5% to δB -10%. The detail of this trend is depicted in Figure 10, in which the flutter velocity is plotted against δB at the nominal value of δH. As δB value decreases, the deck shape becomes less and less aerodynamic, and there is a point (in this case $\delta B \approx$ -5%) where aeroelastic behavior of the box girder rapidly deteriorates. The aeroelastic mode that causes flutter also changes in this design range. It

can also be observed that the optimum δB value occurs at around +5% for the nominal value of δH and the flutter velocity gradually decreases as δB increases.

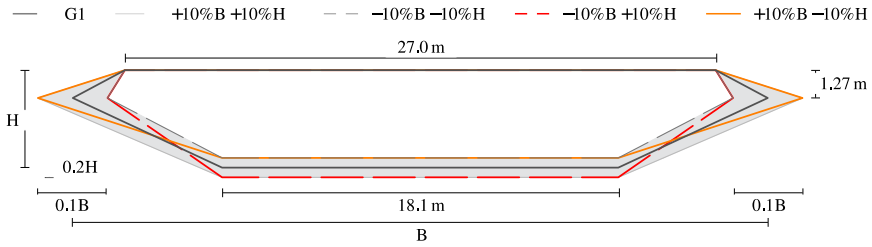

Figure 8. Design domain of different values of *H* and *B*

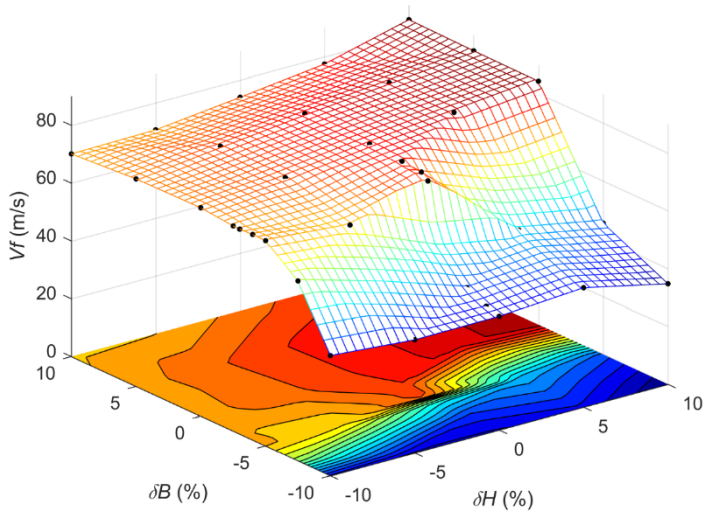

Figure 9. Flutter velocities of different shape variables

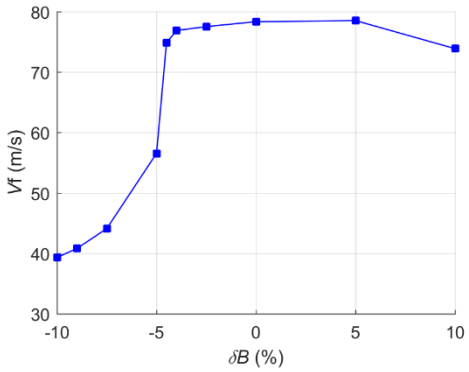

Figure 10. Flutter velocities of different δB values with δH =0 %

5.4 Reliability analysis of the Great Belt East Bridge

The methodology of reliability analysis described in Section 3 was applied to the Great Belt East Bridge. The limit state function that defines the structural failure is already

defined in Eq. (8) while the three force coefficients of C_L, C_D, C_M and their slopes are considered as random variables as well as the extreme wind velocity at the bridge site. The standard deviations of the force coefficients are 20% of their mean values while those for the slopes of the force coefficients are defined in Eq. (6). The extreme wind velocity is a Gumbel distribution function, which is expressed as:

$$f_G(x_i) = \frac{1}{\lambda}\exp(-\frac{x_i-\mu}{\lambda})\cdot\exp\left[-\exp(-\frac{x_i-\mu}{\lambda})\right] \quad (10)$$

where μ=41.60 and λ=2.425. The mean value was taken from the Danish Wind code DS410 (1998) while the standard deviation referred to Storæbelt publication (1998). Since FORM requires that all random variables are normally distributed, the normal-equivalent mean value and standard deviation were computed using Hasofer Lind (1974) – Rackwitz Fiessler method (1976).

Two main cases of reliability analyses were carried out in order to assess the influence of different random variables on overall structural reliability of the suspension bridge. In *Case A*, the extreme wind velocity was considered as a single random variable while in *Case B*, the aerodynamic coefficients and their slopes are added to the random variable of *Case A*.

Reliability analyses were performed on a Linux-based cluster with 848 cores, 10214.4 GFLOP's peak power and total memory of 2624 GB RAM. The termination criteria for all the reliability analyses are defined as the difference of any two consecutive β values to be smaller than 1E-4 and simultaneously the limit state function evaluated at the MPP to be smaller than 1E-4. The results of the reliability analyses are summarized in Table 4.

Table 4. Reliability analysis results

Case	*random var.*	*CV*	β	P_f	V_f(MPP)	V^*(MPP)
A	x_w	0.07	12.01	1.57E-33	78.20	13.22
B	x_w and x_i	0.2	7.42	5.86E-14	61.88	13.09

For *Case A*, only the extreme wind speed is considered as a random variable. Since the limit state function is linear with respect to x_w, β can be directly computed as:

$$\beta = \frac{G(u^*) - \sum_{i=1}^{n} \frac{\partial G(u^*)}{\partial u_i} u_i^*}{\sqrt{\sum_{i=1}^{n} \left(\frac{\partial G(u^*)}{\partial u_i} \right)^2}} = \frac{V_f - \mu_{x_w}}{\sigma_w} = 12.01 \quad (11)$$

In *Case B*, for considering the force coefficients and their slopes as additional random variables, the reliability index has been substantially reduced to 7.42, which indicates the importance of uncertainty in force coefficients. Likewise, the flutter velocity at MPP has been decreased from V_f= 78.2 m/s in *Case A* to 61.88 m/s in *Case B*.

Table 5 shows the initial and MPP values of the random variables for *Case B*. As can be seen, the slopes of lift and moment coefficient C_L and C_M as well as the extreme wind speed have significant influences on overall reliability while the rest of the random variables have little impact. This can be explained by the quasi-steady formulations used to approximate flutter derivatives in this study. According to the theory, the slopes C_L' and C_M' are used to define H^* and A^* flutter derivatives, which are both important flutter derivatives on the computation of flutter velocity. Figure 11 represents the initial and MPP values of the most relevant flutter derivatives for *Case B*. Because of the variations produced mainly in C_L' and C_M' during the reliability analysis, all flutter derivative points have shifted from their initial values. The large shift of A_2^* flutter derivative should be particularly noted because of its significant influence on flutter velocity in general. The points of A_1^* and A_3^* as well as H_2^* flutter derivatives have also considerable displacements from their initial values.

Table 5. Initial and MPP values of the random variables for *Case B*

	C_L	C_D	C_M	C_L'	C_D'	C_M'	*xw*
Initial	-0.0310	0.0580	0.0350	5.4523	0.0048	1.3605	42.473
MPP	-0.0310	0.0570	0.0350	7.0219	0.0040	3.1098	62.092

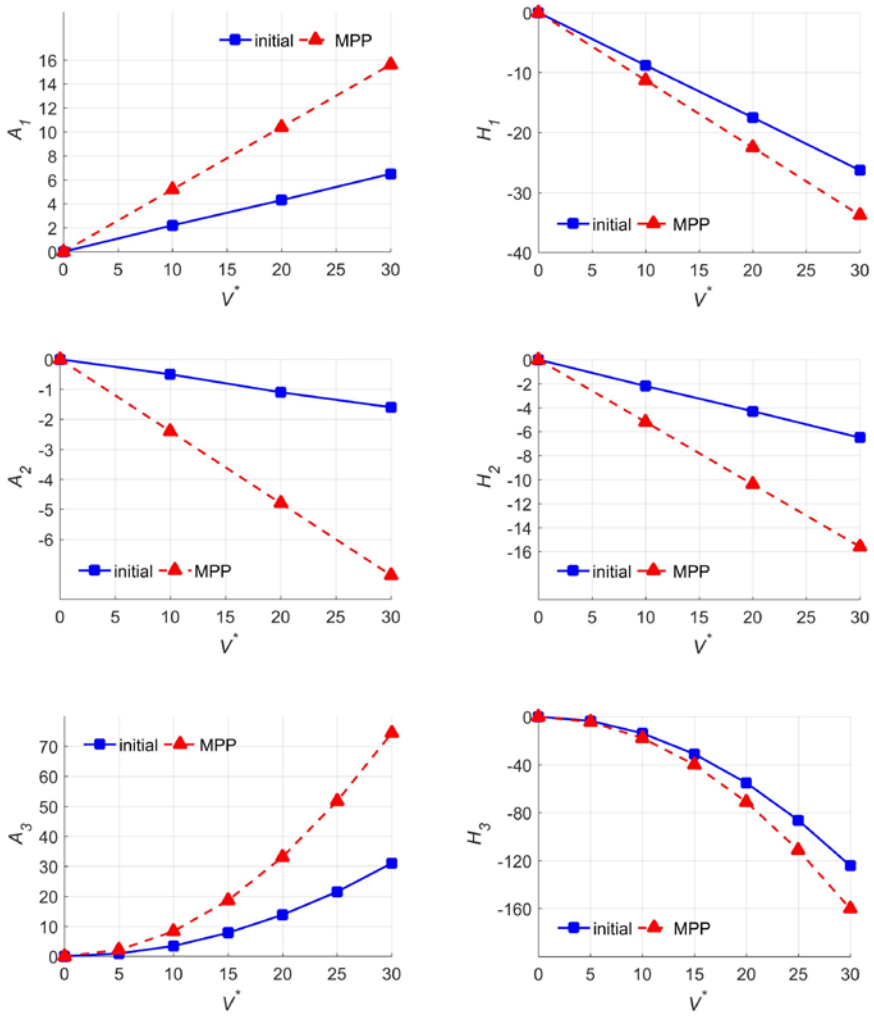

Figure 11. Initial flutter derivatives and their MPP values for *Case B*

5.4.1 Parametric study of reliability index

A parametric study of reliability index was performed with different values of shape variables and the results are summarized in Table 6 and plotted in Figure 12. The reliability index surface has a smooth shape between δB= -2% and δB=+10%; however, it suddenly drops as the deck shape becomes more bluff and less aerodynamic with decreasing value of δB. While maintaining the width at δB=0, the reliability index is largest at the maximum height δH=10% since the stiffness of the girder increases with greater height. On the other hand, for a shorter deck width of δB=-4%, reliability index is largest with δH=-10% since the deck recovers its aerodynamic shape with reduced height.

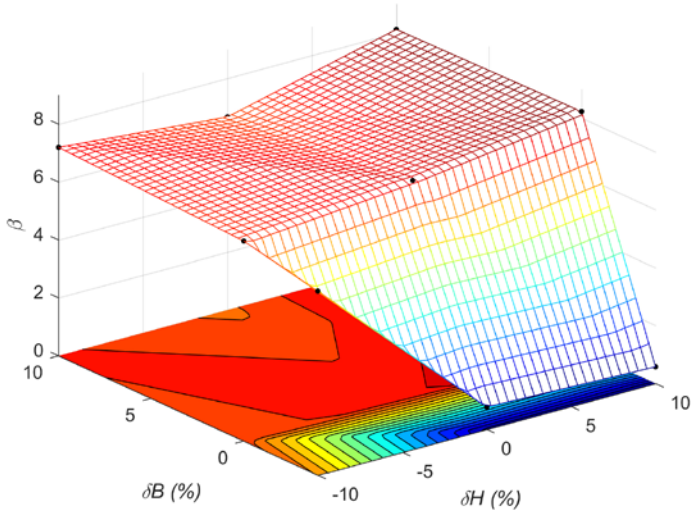

Figure 12. Reliability index β of different shape variables

Table 6. Reliability index β for different shape variables

$\Delta H(\%)$	$\Delta B(\%)$	β
10	10	8.11
0	10	6.67
-10	10	7.2
10	0	8.22
0	0	7.42
-10	0	6.91
10	-4	0.58
0	-4	0.77
-10	-4	6.36

5.5 RBDO of the Great Belt East Bridge

The methodology of RBDO for the shape and the plate thicknesses of box girder of suspension bridges explained in Section 4 is applied to the Great Belt East Bridge in this section. A total of six design variables (Figure 2) are considered in the study, which are two shape variables of $\delta H(\%)$ and $\delta B(\%)$, and the four plate thicknesses that form the aerodynamic box girder while the objective function to be minimized is the material volume of the box girder. Seven random variables of the three force coefficients C_L, C_M and C_D and their slopes as well as the extreme wind speed are taken into account as in the case of reliability analysis with the structural limit state function already defined in Eq. (8). The mean values of the force coefficients and their slopes are taken from the surrogate model based on the shape variables while the standard deviations of the coefficients are defined as CV of 0.2 and those for the slopes in Eq. (6). The statistical data of the extreme

wind velocity can be found in Eq. (10). The detail of the RBDO formulation is explained next.

5.5.1 RBDO formulation of the Great Belt East Bridge

The RBDO problem of the Great Belt East Bridge is formulated as follows:

$$\text{Minimize:} \quad \text{Girder volume } (\delta H, \delta B, d_1, d_2, d_3, d_4) \tag{12a}$$

$$\text{subject to:} \quad g_1 : P\left[V_f(\mathbf{x}) - x_w \le 0\right] \le P_f \tag{12b}$$

$$g_2 : -10\% \le \delta H \le 10\% \tag{12c}$$

$$g_3 : -10\% \le \delta B \le 10\% \tag{12d}$$

$$g_4 : 7 \text{ mm} \le d_j \le 25 \text{ mm} \qquad j = 1, 2, 3, 4 \tag{12e}$$

$$g_5 : \sigma_c = 565 \text{ MPa} \tag{12f}$$

$$g_6 : \frac{z_d}{z_{\max}} - 1 \le 0 \quad \text{where } z_{max}=L/500;\ L=1624 \text{ m} \tag{12g}$$

The shape design variables δH and δB range from -10% to +10% of the original dimension aiming to avoid infeasible shapes for the box girder. The g_6 limits the maximum vertical displacement of the bridge deck under the traffic overload case based on BS 5400 (British Standards Institution, 2000), in which a full load of 2.4 kN/m^2 was applied to the two of the six lanes while 1/3 of the load was applied to the other lanes. The constraint g_5 is used to assign the main cable area whenever the deck weight changes so that the main cable stress is always at 565 MPa. The detail of this constraint is explained next.

Whenever the design of bridge deck changes, the main cable area needs to be modified so that the main cable is always at an acceptable stress value. At first glance, the relationship between the main cable area and the deck weight was not obvious. Naturally, the cable area should increase with greater deck weight; however, any variation in the girder weight alters the initial main cable stress, which modifies the stiffness of the structure. A study was carried out in order to establish the relationship between the deck weight and the cable area, in which 35 finite element analyses were performed under the static overload case by varying the main cable areas and deck weight. The resulting maximum main cable stresses were plotted against the cable areas in Figure 13. Since the maximum main cable stress for the original design under the static overload case described previously was 565 MPa, this stress value was used to determine the main cable

area whenever the deck weight is modified. The relationship between the main cable area A_c and the deck weight W_d was found to be linear as:

$$Ac = 0.0241 \cdot W_d + 0.1046 \quad (13)$$

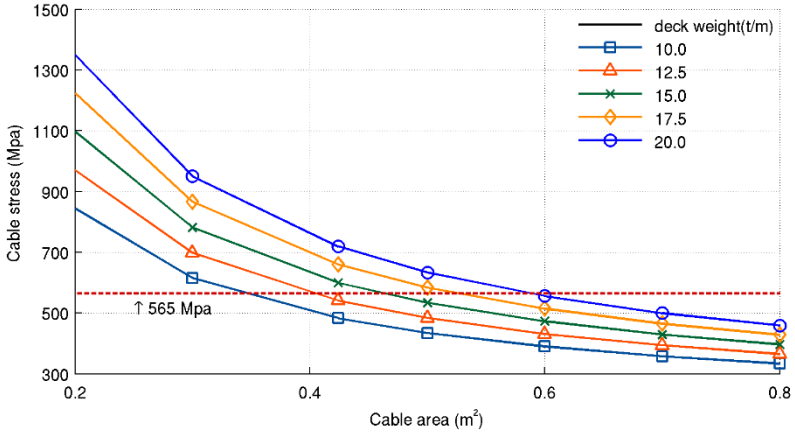

Figure 13. Main cable stress vs. cable area for different deck weight for the Great Belt East Bridge

The RBDO method explained above was programmed in MATLAB (Math Works, 2013), in which the "fmincon" optimizer in MATLAB was employed with active-set algorithm to carry out the optimization routine. The termination criteria of the objective function and the constraint functions was set to 1E-4 while for the reliability routine, any consecutive β values to be smaller than 1.0E-4 and the limit state function evaluated at MPP to be less than 1.0E-4. A high number of FLAS and Abaqus executions are inevitable since the gradients of the objective and constraint functions with respect to each design variable are computed during the optimization process while the derivatives of the limit state function with respect to random variables are calculated during reliability analysis.

The initial design of the deck shape is defined as δH=0%, δB=0% while the plate thicknesses are d_1=12.0, d_2=10.0, d_3=10.0, d_4=10.0 (in mm). The corresponding material volume of the bridge girder is 2779 m^3. The reliability level of the initial design is β = 7.42 (*Case B* in Section 5.4). Several target reliability of β^T=7, 8, 9 and 10 were chosen as predetermined probability of failure to see how the girder design is modified to satisfy different target reliability levels. As a reference, the reliability requirement in Eurocode, EN 1990 (CEN, 2002) for bridges and public buildings is β = 4.3 for 50 year period and β = 5.2 for 1 year period. The primary objective of the study is to achieve the minimum bridge girder volume while satisfying the predetermined reliability level as well as other deterministic structural constraints.

5.5.2 RBDO results

The evolutions of the design variables of shape and plate thicknesses are shown in Figure 14 while the evolution of the objective functions for all cases are represented in Figure 15. Table 7 summarizes the optimum values of the design variables and the objective functions.

For all cases, the shape variable of height δH goes to the maximum value of +10% to increase the stiffness of the deck while the aerodynamic performance of the deck is not compromised. On the other hand, the shape variable δB varies between -0.32 to 4.51 % without presenting any correlation with the target β. Recall from Figure 12, the 3D plot of the reliability indices for different shape variable, the β value is rather insensitive in this range of δB presenting almost a flat area in the plot. As long as δB does not fall in the range below approximately -2% where β drops suddenly for losing the aerodynamic shape, δB value in this range has little impact on the constraint function for this particular example.

For a target reliability of β^T=6.0, all design variables of the plate thicknesses have decreased close to the minimum while as the target reliability value increases, the optimum design variable values are more dispersed. For requiring a target reliability of β^T=7, slightly reduced from the reference reliability index of β=7.58 of the initial design, the girder volume was reduced by 16.8% and even for slightly larger target reliability of β^T=8, the objective function was reduced by 7%. On the other hand, for a larger target reliability of β^T=9 from the initial design, the girder volume has increased by 7.01% while for β^T=10, it has augmented by 21.38%. The optimum objective function values are in accordance with the required target reliability as expected.

Table 8 lists the critical flutter velocity and the reduced velocity at which flutter occurs as well as the first vertical and torsional frequencies for the optimum design for each target β. The critical flutter velocity of the optimum increases with the target beta and so does the frequency ratio. This means that the increase in critical flutter velocity comes largely from the structural contribution of thicker steel plates as well as the deck shape. While the first vertical frequency is almost constant, the first torsional frequency steadily increases with larger β^T. This is because the optimization algorithm modifies to increase the torsional frequency, which is very effective to augment the critical flutter velocity.

The computational time to obtain the optimum design for each target reliability is summarized in Table 9. The computation was carried out using a series of CPU for the design optimization and reliability analysis using Matlab codes while Abaqus static and modal analyses were performed in parallel. The high computational time was mainly due to the high numbers of FLAS executions to compute critical flutter velocity during the reliability analysis. The high computational time for β^T=10 is due to the difficulties of convergence in reliability analysis.

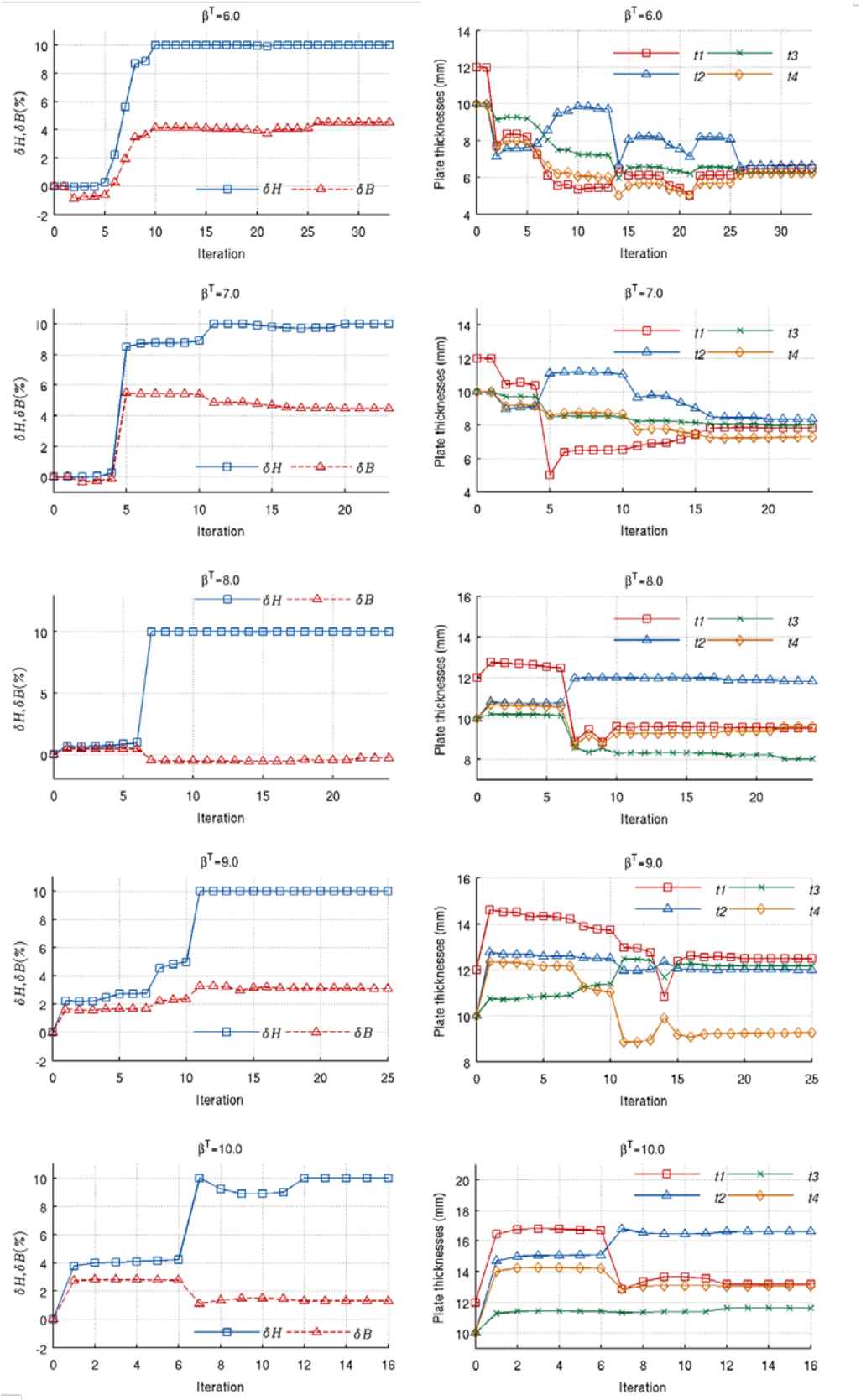

Figure 14. Evolution of the shape and plate thicknesses for different β^T values

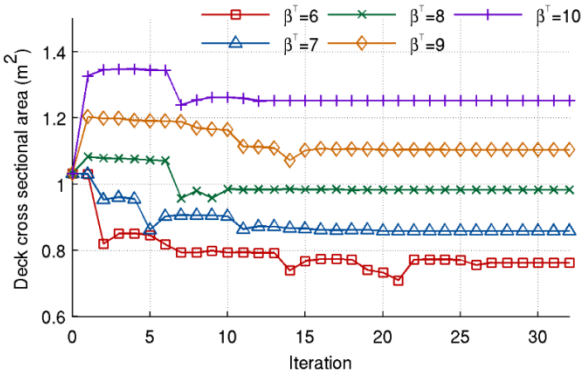

Figure 15. Evolution of objective functions for different β^T values

Table 7. RBDO results for different target reliability

β^T	V_f	δH	δB	d_1	d_2	d_3	d_4	*obj. func.*	*% variation obj. func.*
6	69.45	10.00	4.51	6.48	6.63	6.24	6.24	2054.93	-26.07
7	75.09	10.00	4.48	7.81	8.35	7.98	7.26	2313.63	-16.77
8	82.10	10.00	-0.32	9.51	11.82	8.02	9.58	2647.45	-4.76
9	86.95	10.00	3.10	12.49	12.00	12.16	9.25	2974.45	7.01
10	92.70	10.00	1.31	13.17	16.62	11.61	13.06	3373.97	21.38

Table 8. Flutter velocity and ratio of the 1st torsional frequency to the 1st vertical frequency of the optimum designs for each β^T

β^T	V_f	V^*	1st vert. freq.	1st tor.freq.	ratio
6	69.45	11.96	0.6199	1.7643	2.846
7	75.09	13.15	0.6204	1.8132	2.923
8	82.10	13.47	0.6216	1.8723	3.012
9	86.95	15.18	0.6209	1.8744	3.019
10	92.70	16.06	0.6222	1.9126	3.074

Table 9. Computational time and the number of FLAS executions

β^T	*No. FLAS executions*	*compt. time (hrs)*
6	50,953	549
7	63,840	673
8	55,706	662
9	64,547	776
10	70,056	865

6 Conclusions

The RBDO for shape and size optimization of a single-box girder of suspension bridges was performed considering probabilistic flutter constraint, and this methodology

was applied to the Great Belt East Bridge with G1 deck section as a base geometry. The entire process of the RBDO was carried out using fully numerical approach including the definition of flutter derivatives. A surrogate model was used to estimate the aerodynamic force coefficients for different deck shapes based on the CFD simulations.

Reliability level of the initial design was computed to be β=7.42 by taking into account uncertainty in the aerodynamic force coefficients and their slopes as well as the extreme wind velocity at the bridge site. The resulting MPP values indicate the importance of the slopes of lift and moment coefficients in the bridge flutter, which can be verified by the quasi-steady formulation. The parametric study of reliability index with respect to the shape variables show that the larger δH produces better reliability index in this study whenever the aerodynamic deck shape is maintained.

As a result of the RBDO of the bridge deck for several target reliabilities, the optimum shape design variable δH reached its maximum value of +10% for all cases to increase the stiffness of the deck. The optimum width variable δB varies between -0.32 to 4.51 % with respect to the initial dimension since reliability index in this range is not sensitive to this parameter for this particular case. During the optimization process, once the deck shape is established, the algorithm either reduces or increases the plate thicknesses depending on the required target reliability β^T. The optimum plate thicknesses for small β^T are clustered together near lower design limit while for larger β^T, they are more scattered. The increasing first vertical to torsional frequency ratio with larger β^T indicates the importance of structural contribution of thicker steel plates and the deck shape to critical flutter velocity and consequently, to the reliability of bridge flutter.

The high computational cost for all cases in this study should be improved using parallel computing and other RBDO methods in the future research. Also design constraints of other relevant wind-induced vibrations such as buffeting and vortex-induced vibration will be included in the forthcoming works of design optimization of bridge deck shape for cable-supported bridges.

Acknowledgements

This research was financed by the Spanish Ministry of Economy under project BIA2016-76656R.

7 References

Abaqus Inc. (2015) Abaqus v6R2016

Argentini, T., Pagani, A., Zasso, A. (2014) Monte Carlo analysis of total damping and flutter speed of a long span bridge: effects of structural and aerodynamic uncertainties. J. Wind Eng. Ind. Aerodyn 128, 90-104.
Arora, J. (2016) Introduction to Optimum Design. Academic Press
Belloli, M., Fossati, F., Giappino, S. and Muggiasca, S. (2014) Vortex induced vibrations of a bridge deck: Dynamic response and surface pressure distribution. J. Wind Eng. Ind. Aerodyn. 133, 160-168
Baldomir, A., Kusano, I., Jurado, J.A., Hernández S. (2013) A reliability study for the Messina Bridge with respect to flutter phenomena considering uncertainties in experimental and numerical data. Computers and Structures, 128, 91-100
Bruno, L. and Fransos, D. (2011) Probabilistic evaluation of the aerodynamic properties of a bridge deck. J. Wind Eng. Ind. Aerodyn. 99: 718-728.
British Standards Institution (2000) British Standard code of practice for steel, concrete and composite bridges. BS 5400-3
Caracoglia, L. (2009) Effects of non-linear propagation of random turbulence fields on bridge flutter instability. J. Wind Eng. Ind. Aerodyn. 99(9) 945-954
Cheng, J., Cai, C.S., Xiao, R., Chen, S.R. (2005) Flutter reliability analysis of suspension bridges. J. Wind Eng. Ind. Aeodyn. 93 (10) 757-775 2005
Cheng, J. and Li, Q.S. (2009) Reliability analysis of long span steel arch bridges against wind-induced stability failure. J. Wind Eng. Ind. Aerodyn. 97 132-139
Cid Montoya, M., Nieto, S., Hernández, S., Kusano, I., Álvarez, A.J., Jurado, J.A. (2018) CFD based aeroelastic characterization of streamlined bridge deck cross-sections subject to shape modifications using surrogate models. J. Wind Eng. Ind. Aerodyn. 177 405-428
Cid Montoya, M., Hernández, S., Nieto, F. (2018) Shape optimization of streamlined decks of cable-stayed bridges considering aeroelastic and structural constraints. J. Wind Eng. Ind. Aerodyn. 177 429-455
Danish Standard Association (1998) Danish Wind Code SD410. Copenhagen, Denmark
Diana, G., Fiammenghi, G., Belloli, M. and Rocchi, D. (2013) Wind tunnel tests and numerical approach for long span bridges: The Messina bridge. J. Wind Eng. Ind. Aerodyn. 122, 38-49
Diana G, Stoyanoff S, Aas-Jakobsen k, Allsop A, Andersen M, Argentini A, Cid Montoya M, Hernández S, Jurado JA, Katsuchi H, Kavrakov I, Kim H-K, Larose G, Larsen A, Morgenthal G, Oiseth O, Omarini S, Rocchi D, Svendsen M and Wu T (2019). IABSE Task Group 3.1 benchmark results. Part 1: Numerical analysis of a 2-degree-of-freedom bridge deck section based on analytical aerodynamics. Structural Engineering International (IABSE), DOI: 10.1080/10168664.2019.1639480
Díaz, J., Cid Montoya, M., Hernández, S. (2016) Efficient methodologies for reliability-based design optimization of composite panels. Advances in Engineering Software 93:9–21.
European Committee for Standardization (CEN) (2002) Eurocode – Basis of structural design: EN 1990
Forrester, A.I.J., Sóbester, A., Keane, A.J., (2008) Engineering Design via Surrogate Modelling. Wiley.
Forrester, A.I.J. and Keane, A.J. (2009) Recent advances in surrogate-based optimization. Prog. Aero. Sci. 45, 50–79.
Ge, Y.J., Xiang, H.F. and Tanaka, H. (2000) Application of a reliability analysis model to bridge flutter under extreme winds. J. Wind Eng. Ind. Aerodyn. 86(2-3) 155-167.
Ge, Y. J., and H. F. Xiang. (2008) Recent development of bridge aerodynamics in China. J. Wind Eng. Ind. Aerodyn. 96.6-7, 736-768
Ge, Y.J. (2016) Aerodynamic challenge and limitation in long-span cable-supported bridges. World Congresson Advances in Civil, Environmental, and Materials Research. Jeju Island, Korea
Gimsing, N. J. and Georgakis C. T. (2012). Cable Supported Bridges: Concept and Design. John Wiley & Sons Ltd., 3. edition.
Gorlé, C., Garcia-Sanchez, C., Iaccarino, G. (2015) Quantifying inflow and RANS turbulence model form uncertainties for wind engineering flows. J. Wind Eng. Ind. Aerodyn, 144:202–212
Hasofer, A. M. and Lind, N. (1974) An exact and invariant first-order reliability format. Journal of the Engineering Mechanics Division, 100(EM1) 111–121
Hernandez, S. (1990) Métodos de diseño óptimo de estructuras. Colegio de Ingenieros de Caminos, Canales y Puertos
Jurado, J.A., Hernánsez, S. (2004) Sensitivity analysis of bridge flutter with respect to mechanical parameters of the deck. Structural Multidisciplinary Optimization 27:272-283
Jurado, J.A., Hernandez, S., Nieto, F. and Mosquera, A. (2011) Bridge Aerolasticity: Sensitivity Analysis and Optimal Design. WIT press
Jurado, J.A., Kusano, I., Hernandez, S., Nieto, F. (2013) Improvement of multimodal flutter analysis code, FLAS. CWE2013, Cambridge, UK.

Kareem, A. (1988). Effect of parametric uncertainties on wind excited structural response. J. Wind Eng. Ind. Aerodyn. 30:233-241.
Katsuchi, H., Jones, N.P., Scanlan, R.H. (1999) Multimode coupled flutter and buffeting analysis of the Akashi-Kaikyo Bridge. J. Struct. Eng. 125 (1), 60-70
Karadeniz, H., Toğan, V., Vrouwenvelder, T. (2009) An integrated reliability-based design optimization of offshore towers. Reliability Engineering & System Safety Volume 94, Issue 10, 1510-1516
Kusano, I., Baldomir, A., Jurado, J.A., Hernández, S. (2014) Reliability based design optimization of long-span bridges considering flutter. J. Wind Eng. Ind. Aerodyn, 135:149–162
Kusano, I., Baldomir, A., Jurado, J.A., Hernández, S. (2015) Probabilistic optimization of the main cable and bridge deck of long-span suspension bridges under flutter constraint. J. Wind Eng. Ind. Aerodyn. 146, 59-70
Kusano, I., Baldomir, A., Jurado, J.A., Hernández, S. (2018) The importance of correlation among flutter derivatives for the reliability based optimum design of suspension bridges. Engineering Structures 173, 416-428.
Krige, D.G. (1951) A statistical approach to some basic mine valuation problems on the Witwatersrand. Journal of the Southern African Institute of Mining and Metallurgy 52(6), 119-139.
Larose, G. L. and Livesey, F. M. (1997) Performance of streamlined bridge decks in relation to the aerodynamics of a flat plate. J. Wind Eng. Ind. Aerodyn. 69-71 851-860
Larsen, A. (1993) Aerodynamic aspects of the final design of the 1624 m suspension bridge across the Great Belt. J. Wind Eng. Ind. Aerodyn. 48 261-285
Larsen, A. and Walther, J. H. (1998) Discrete vortex simulation of flow around five generic bridge deck sections. J. Wind Eng. Ind. Aerodyn. 77-78:591-602.
Larsen, A. and Wall, A. (2012) Shaping of bridge box girders to avoid vortex shedding response. J. Wind Eng. Ind. Aerodyn. 104-106, 159-165

Lazzari, M. (2005) Time domain modelling of aerlastic bridge decks: a comparative study and an application. International Journal for Numerical Methods in Engineering, 62:1064–1104, 2005.
Liu, T. T., Xu, Y. L., Zhang, W. S., Wong, K. Y., Zhou, H. J., Chan, K. W. Y. (2009) Buffeting-induced stresses in a long suspension bridge: structural health monitoring oriented stress analysis. Wind and Structures, 12(6): 479–504
Martins Gomes, H. and Awruch, A. M. (2004) Comparison of response surface and neural network with other methods for structural reliability analysis. Structural Safety 26:49–67.
Martins Gomes, H., Awruch, A. M., Menezes Lopes P. A. (2011) Reliability based optimization of laminated composite structures using genetic algorithms and Artificial Neural Networks. Structural Safety 33:186–195.
Mavris, D.N., Bandte, O., DeLaurentis, D.A. (1999) Robust Design Simulation: A Probabilistic Approach to Multidisciplinary Design, Journal of Aircraft, Vol. 36, No. 1. 298-307.
MathWorks Inc. (2013) MATLAB 8.1. Natick, MA, USA
Nikolaidis, E. and Burdisso, R. (1988) Reliability based structural optimization: a safety index approach. Computer and Structures 28 (6) p.781-788
Ostenfeld-Rosenthal, P., Madsen, H.O., Larsen, A. (1992) Probabilistic flutter criteria for long-span bridges. J. Wind Eng. Ind. Aerodyn. 42(1-3) 1265-1276
Pagnini L. (2010) Reliability analysis of wind-excited structures. J. Wind Eng. Ind. Aerodyn. 98:1-9.
Pourzeynali S. and Datta T.K. (2002) Reliability analysis of suspension bridges against flutter. Journal of Sound and Vibration 254(1):143-162.
Rackwitz, R. and Fiessler, B. (1976) Note on discrete safety checking when using non-normal stochastic models for basic variables. Load Project working session, MIT, MA.
Rojiani K. and Wen Y K (1981) Reliability of Steel buildings under wind. Proc. ASCE, J. Structural Division 107(ST1):203-221.
Sacks, J., Welch, W.J., Mitchell, T.J., Wynn, H. (1989) Design and analysis of computer experiments. Stat. Sci. 4 (4), 409–423.
Sarkar, P., Caracoglia, L., Haan Jr., F., Sato, H., Murakoshi, Jun. (2009) Comparative and sensitivity study of flutter derivatives of selected bridge deck sections, Part 1: Analysis of inter-laboratory experimental data. Engineering Structures 31, 158-169
Scanlan, R.H. and Tomko, J.J. (1971) Airfoil and bridge deck flutter derivatives. Journal of Engineering Mechanics Division 97(6):1717–1737
Seo, D.W. (2013) Effects of errors in flutter derivatives on the wind-induced response of cable-supported bridges. Dissertation, Northeastern University.
Shueller G.I., Hirtz, H., Booz, G. (1983) The effect of uncertainties in wind load estimation on reliability assessments. J. Wind Eng. Ind. Aerodyn. 14:15-26

Simpson T. W. and Mistree F. (2001) Kriging models for global approximation in simulation-based multidisciplinary design optimization. AIAA Journal 39(12):2233-2241

Solari G. and Piccardo G. (2001) Probabilistic 3-D turbulence modeling for gust buffeting of structures. Probabilistic Engineering Mechanics 16:73-86.

The Storebælt publication. (1998) East Bridge Denmark

Thomas, C., Caracoglia, L., and Denoël, V. (2015) Application of random eigenvalue analysis to assess bridge flutter probability. J. Wind Eng. Ind. Aerodyn. 140, 79-86.

Su, C., Luo, X., Yun, T. (2010) Aerostatic reliability analysis of long-span bridges Journal of Bridge Engineering 15, Issue 3 260-268

Tubino, F. (2005) Relationship among aerodynamic admittance functions, flutter derivatives and static coefficients for long-span bridges. J Wind Eng. Ind. Aerodyn. 93, 929–950

Wu, T. and Kareem, A. (2013) Bridge aerodynamics and aeroelasticity: A comparison of modeling schemes. Journal of Fluids and Structures 43:347–370.

Xu, Y.L., Liu, T.T. and Zhang, W.S. (2009) Buffeting-induced fatigue damage assessment of a long suspension bridge. J. Wind Eng. Ind. Aerodyn. 31, 575-586

Yao, W., Chen, X., Luo, W., Van Tooren, M., Guo, J. (2011) Review of uncertainty-based multidisciplinary design optimization methods for aerospace vehicles. Progress in Aerospace Sciences. 47 (6) 450-479

Youn, B., Choi, K., Yang, RJ. (2004) Reliability-based design optimization for crashworthiness of vehicle side impact. Struct Multidisc Optim 26: 272

Zhu, Q., Xu, Y.L. and Shum, K.M. (2016) Stress-level buffeting analysis of a long-span cable-stayed bridge with a twin-box deck under distributed wind loads. Eng. Structures 127, 416-433